$$\text{difference of PSF} = \frac{1}{N}\sum_{i}^{N}\left\{\left(\text{width of PSF}_{\text{measured}}\right)_i - \left(\text{width of PSF}_{\text{computed}}\right)_i\right\} \quad (7)$$

Simulation of Light Scattering

To determine the angular characteristics of Mie scattering by spherical particles, a rigorous solution exists. The theory and a program to compute it are well documented in a textbook,[26] and ready-to-use programs are even available on the Internet.[27] Here, we comment briefly on the theory of Mie scattering. Because Mie scattering concerns scattering by a spherical particle, the coordinate system chosen is spherical polar coordinates. We can find a solution of the wave equation of an electromagnetic field in spherical polar coordinates by using the method of separation of variables. After finding the form of the solution equation, we need to find a solution that satisfies the boundary conditions at the surface of the spherical particle. We need an efficient numerical method to calculate the final solution with a personal computer.

Such a method has been developed.[26] The size of the particle and refractive indices outside and inside the particle are important parameters in the analysis. The sizes of the particles used were 0.7 μm and 4 μm. These are typical sizes of particles that induce Mie scattering in a crystalline lens.[28,29] In this study, we were interested in the scattering of the measurement light of the Hartmann-Shack wavefront sensor. We used a wavelength of 840 nm and unpolarized light for the calculation. The ratio of the refractive indices between the particle and its surroundings was 1.1.[29,30]

Angular characteristics from diffraction and aberration were evaluated with equation 4. The PSF on the fundus was simulated using this equation. In this simulation, Zernike coefficients of one of the keratoconic eyes in the study with the largest aberrations were used.

Data Analysis

All statistical tests were carried out with the software package Statview Version 5.01 (SAS Institute, Cary, NC, USA) or SPSS Version 12 (SPSS, Chicago, IL, USA). We used 95% confidence limits.

Results

Wavefront Aberrations

The RMS value of third- and fourth-order wavefront aberrations in a 4-mm pupil area was 0.078 ± 0.044 μm (mean ± SD) for the normal eyes, 0.347 ± 0.239 μm for the keratoconic eyes, and 0.230 ± 0.098 μm for the cataractous eyes. A statistically significant difference was found among those three groups [analysis of variance (ANOVA), $DF = 2$, $F = 7.119$, $P = 0.0021$). However, a statistically significant difference was found only between normal and keratoconic eyes in the post hoc test (Scheffé test, *Mean Diff* = 0.268 μm, $P = 0.0027$).

Contrast Method

Figure 5 shows the results of the image contrast measurements. In each graph, the horizontal axis represents the magnitude of third- and fourth-order wavefront aberrations, and the vertical axis is the inverse of the image contrast. As the inverse of the image contrast was used to represent the light scattering quantitatively, a larger value represents a larger degree of light scattering.

The inverse of contrast in the 4-mm pupil area was 1.57 ± 0.56 (mean ± SD) for the normal eyes, 1.83 ± 0.79 for the keratoconic eyes, and 5.04 ± 3.06 for the cataractous eyes. Among them, a significant statistical difference was found (ANOVA, $DF = 2$, $F = 15.554$, $P < 0.0001$).

The inverse contrast of cataractous eyes was significantly larger than those of normal eyes (Scheffé test, *Mean Diff* = 3.467, $P = 0.0007$) and of keratoconic eyes (Scheffé test, *Mean Diff* = 3.205, $P < 0.0001$), while the inverse contrast of normal eyes and that of keratoconus eyes were not significantly different (Scheffé test, *Mean Diff* = 0.262, $P = 0.9479$).

There was no significant correlation between inverse contrast and third- and fourth-order wavefront aberrations for keratoconic eyes ($r = 0.087$, $P = 0.700$) or cataractous eyes ($r = 0.142$, $P = 0.587$).

We linearly transformed the two axes in Fig. 5a or b to the canonical discriminant functions in Fig. 5c for better separation. Using the squared Mahalanobis distance between each sample point and the group centroid, the analysis classified 84.0% of the originally grouped cases correctly. We used separate group covariance matrices for the canonical discriminant functions. Results are shown in Table 1.

PSF Method

Figure 6 shows the relation between the scattering that was calculated with equation 6 and the third- and fourth-

Table 1. Classification results after discriminant analysis with SPSS of contrast method data

Eye type	Normal region	Keratoconic region	Cataractous region
Normal	8 (100%)	0 (0%)	0 (0%)
Keratoconic	3 (12%)	19 (76%)	3 (12%)
Cataractous	1 (6%)	1 (6%)	15 (88%)

84.0% of originally grouped cases were correctly classified.

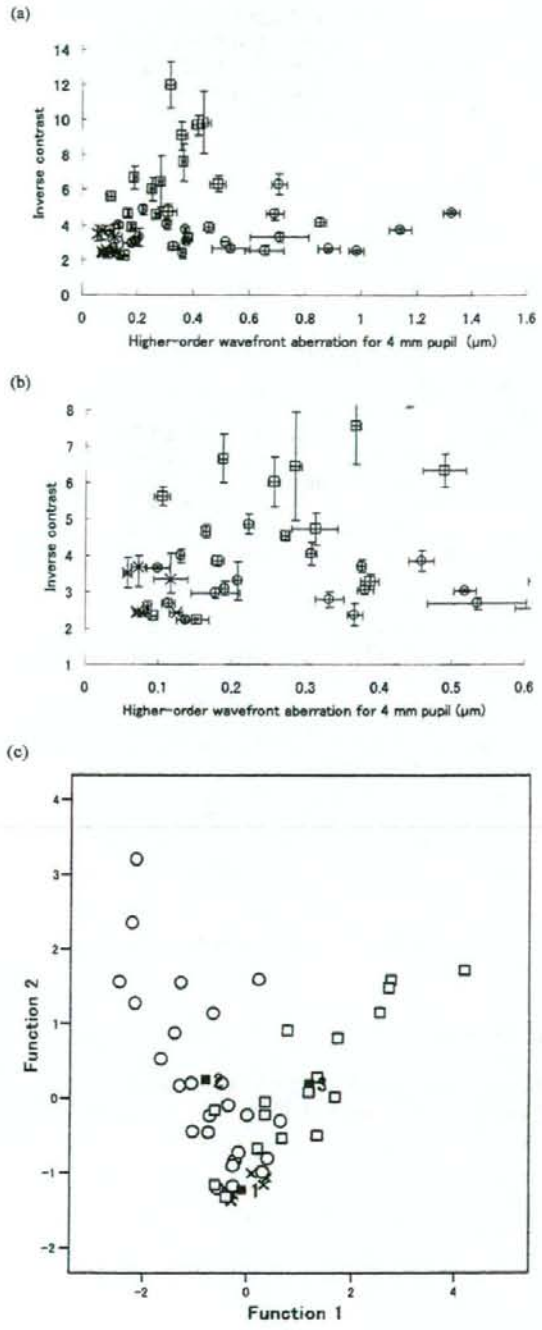

Table 2. Classification results after discriminant analysis with SPSS of difference of PSF data

Eye type	Normal region	Keratoconic region	Cataractous region
Normal	8 (100%)	0 (0%)	0 (0%)
Keratoconic	2 (8%)	17 (68%)	6 (24%)
Cataractous	1 (6%)	2 (12%)	14 (82%)

78.0% of originally grouped cases were correctly classified
PSF, point spread function

order wavefront aberrations. All data values except one (=–0.96 μm) were positive.

The difference in PSFs in the 4-mm pupil area was 9.3 ± 4.3 μm (mean ± SD) for the normal eyes, 30.0 ± 20.1 μm for the keratoconic eyes, and 81.8 ± 65.2 μm for the cataractous eyes. A statistical difference was found among them (ANOVA, $DF = 2$, $F = 10.983$, $P = 0.0001$).

The difference in the PSFs of cataract eyes was significantly larger than that of normal eyes (Scheffé test, *Mean Diff* = 73, $P = 0.0009$) or keratoconic eyes (Scheffé test, *Mean Diff* = 52, $P = 0.0017$), while those of normal eyes and keratoconus eyes were not significantly different (Scheffé test, *Mean Diff* = 21, $P = 0.4911$).

There was no significant correlation between the differences of PSF and the third- and fourth-order wavefront aberrations: $r = 0.328$ ($P = 0.136$) for keratoconic eyes and $r = 0.309$ ($P = 0.227$) for cataractous eyes.

Again, we linearly transformed the two axes of Fig. 6a or b to the canonical discriminant functions in Fig. 6c for better separation. Using the squared Mahalanobis distance between each sample point and the group centroid, the analysis classified 78.0% of the originally grouped cases correctly. Results are shown in Table 2.

Simulation of Light Scattering

Results of Mie scattering simulations are shown in Fig. 7. The half-width at half height of the scattering function by a 0.7-μm particle is 18.8° and that for a 4-μm particle is 2.8°.

Simulations of diffraction and wavefront aberration are shown in Fig. 8. The half-width at half height of the PSF for a keratoconic eye was 0.02°, which was much narrower than that of the scattering from the particles.

Figure 5a–c. Light scattering evaluated by the contrast method. The horizontal axis is the RMS of third- and fourth-order wavefront aberrations for the central 4-mm pupillary area. The vertical axis is the inverse contrast. Normal eyes (×), keratoconic eyes (○), and cataractous eyes (□) are shown. Error bars designate standard errors. **a** and **b** are the same graph but **b** is expanded to show small values clearly. **c** Graph with canonical functions generated by an SPSS discrimination analysis. Data were divided into three groups so that each data point has the smallest Mahalanobis distance between its position and the corresponding group centroid. ■1 is the centroid of the normal group, ■2 is that of the keratoconic group, and ■3 is that of the cataractous group.

Jpn J Ophthalmol
Vol 50: 323–333, 2006

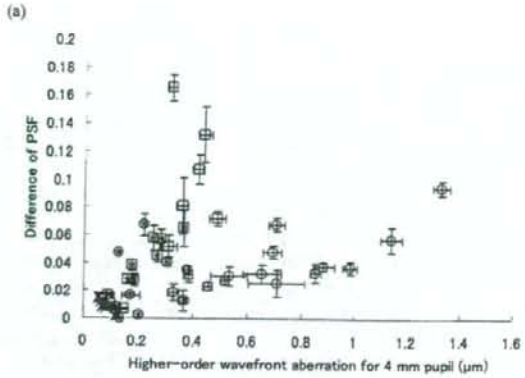

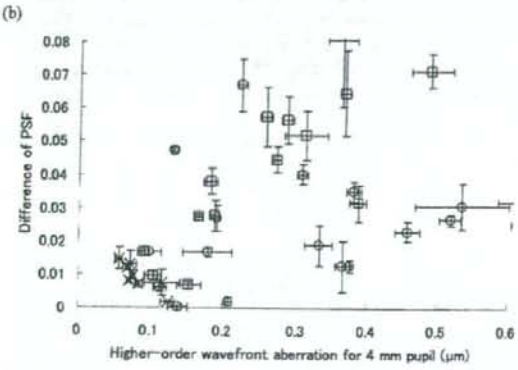

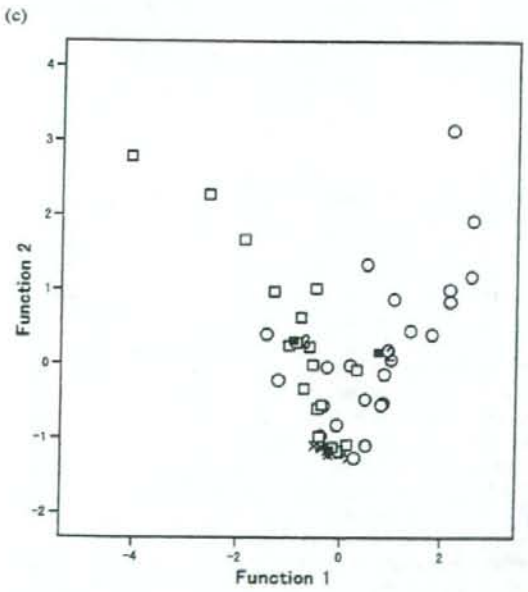

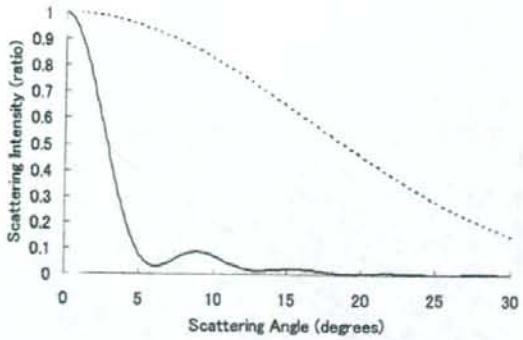

Figure 7. Angle dependency of Mie scattering by 0.7-μm particles (dashed line) and 5-μm particles (solid line) calculated using MiePlot.

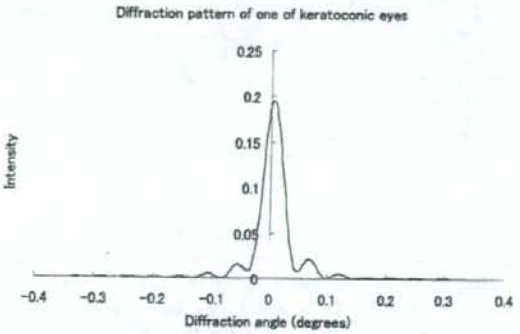

Figure 8. Angle dependency of aberrations and diffraction. The PSF was obtained by a Fourier transform of pupil function.

Comparison Between the Contrast and PSF Methods

The values of light scattering estimated by the contrast method and those estimated by the PSF method were highly correlated ($r = 0.893$, $P < 0.0001$) (Fig. 9).

Discussion

In this study, we investigated intensity measurement of Hartmann-Shack images and developed two different methods, the contrast method and the PSF method. The two methods were in agreement in that a greater numerical

Figure 6a–c. Light scattering evaluated by the point spread function (PSF) method. The horizontal axis is the RMS of third- and fourth-order wavefront aberrations for the central 4-mm pupillary area. The vertical axis is the difference in width (μm) between the computed PSF and the measured PSF. Normal eyes (×), keratoconic eyes (○), and cataractous eyes (□) are shown. Error bars designate standard errors. **a** and **b** are the same graph but **b** is expanded to show small values clearly. **c** The result of an SPSS discriminant analysis, as in Fig. 5.

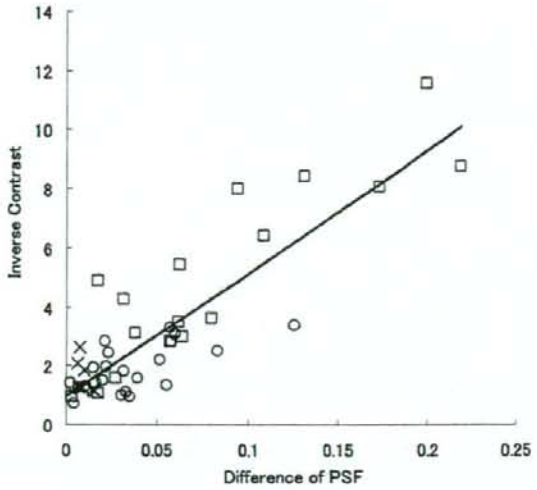

Figure 9. Correlation between the light scattering values estimated by the contrast method and that estimated by the PSF method. The horizontal axis is the difference in width between the two PSFs, and the vertical axis is the inverse contrast. Normal eyes (×), keratoconic eyes (○), and cataractous eyes (□) are shown.

value was found in cataractous eyes than in normal or keratoconic eyes. For cataractous eyes, in which the light scattering due to the cataracts predominates over the aberrations, no correlation was found between the third- and fourth-order aberrations and the results of the inverse contrast or PSF methods (Figs. 5, 6), suggesting that neither results were related to the third- and fourth-order wavefront aberrations. For the keratoconic eyes, in which the aberration is the major cause of the blurred PSF, again no correlation was found between the third- and fourth-order aberrations and the results of the inverse contrast or PSF methods. This finding also suggests that the third- and fourth-order aberrations did not influence the results from the two methods. These findings are in agreement with those of a previous study.[31]

The characteristics of light scattering depend on the size and the density of the particles. If the size of the particles is much smaller than the wavelength of the light, less angle-dependent and wavelength-dependent Rayleigh scattering is observed. If the size of the particles is comparable to or not much larger than the wavelength of the light, angle-dependent but not wavelength-dependent Mie scattering should be observed. If the particles are huge, scattering can be described by geometrical optics. van den Berg and Spekreijse[32] investigated the size of the particles by measuring light scattering from donor lenses with several wavelengths of light and several angles of scattering. They concluded that the scattering is Rayleigh-Ganz scattering and that the size of the particles that were the source of the scattering was 0.76 μm (median = 0.76, range, 0.55–1.02 μm, from Table 2 of their study).[32] Scattering can be rigorously calculated from the size of spherical particles by Mie approximation. Using an electron microscope, Gilliland et al.[29] concluded that scattering from a crystalline lens includes Mie scattering and the size of the scattering source was from 1 to 4 μm.[29] We recalculated the angle characteristics of Mie scattering for 0.7-μm and 4-μm particles and the results are shown in Fig. 7.

In the contrast method, we evaluated Michelson contrast around each bright spot in the Hartmann-Shack image. Michelson contrast is the ratio of the maximum–minimum intensity difference to the sum of the maximum and minimum intensities. The angular spread of the PSF by the diffraction and wavefront aberration with up to fourth-order terms measured by classical wavefront sensing for one of the most aberrated keratoconic eyes in this study is shown in Fig. 8. This spread should not affect the minimum intensity of the area selected to evaluate the contrast. In contrast, from Fig. 7, the light scattering from the 0.7-μm particles or 4-μm particles affects the entire area corresponding to the square in Fig. 3, and thus raises the minimum intensity.

In the case of the PSF method, we cannot explain the results by Mie scattering from these 0.7-μm or 4-μm particles because the blur around the PSF was at a much lower angle than those of the Mie scattering. The angular distributions of the intensity for third- and fourth-order aberrations and diffraction (Fig. 8) are much narrower than those for the Mie scattering (shown in Fig. 7). Finding the exact cause of this very low angle scattering will require a new method of measurement and another full study. Here, we are just speculating about the cause. A possible cause is larger particles or higher order aberrations, higher than fourth order. Also, we have occasionally observed a very quick change of the pattern and color in retroillumination images of the crystalline lens (for example, Fig. 5 in reference 14), which may be related to spatial characteristics of the variation in the extinction rate or to the spatial distribution of the refractive index. The edge of the spatial distribution could cause light scattering.[33]

One of the interesting results from this study is that the values of light scattering estimated with the contrast and PSF methods showed a good correlation ($r = 0.893$, $P < 0.0001$) (Fig. 7). As we mentioned, the two kinds of light scattering we observed in the two methods might be caused by different sources. Good correlation of the results suggests that the strengths of the sources were well correlated. Because the number of subjects in this study was limited and not only cataractous but also normal and keratoconic eyes were included in the estimate of the correlation, we need further study to confirm this.

The wavelength of the measurement was 840 nm, which was near infrared light instead of visible light (400–800 nm). It is well known that light scattering is wavelength-dependent. In particular, light scattering caused by small particles is more wavelength-dependent than that caused by larger particles. In our methods, mainly forward light scattering was measured. At a low angle (less than 10°), light scattering from a crystalline lens is dominated by larger particles

(Fig. 2 in the study of van den Berg and Spekreijse).[32] From this study and other literature,[33] scattering from larger particles is less wavelength-dependent than that from small particles. Also, the near infrared wavelength was close to red visible light and the size of particles varied, so we believe that we can reasonably infer that forward light scattering from the crystalline lens was measured with infrared light.

The blur might also be caused by scattering in the retina. However, in our results for normal eyes, the measured PSFs were not larger than the computed PSFs. This means that the normal retina does not generate scattering, which would affect the PSF method, in carefully chosen subjects. In this study, we clinically chose subjects whose eyes did not have any retinal pathology. Hence, retinal scattering was not a factor in the PSF method.

The results of the discriminant analysis show the possibility of categorization. The two- dimensional maps with inverse contrast and the third- and fourth-order aberrations, and with a difference in PSF and the aberrations, also graphically show the possible categorization of the optical degradation in the eye (Figs. 5a, b and 6a, b). Eyes with large optical aberrations and small light scattering, such as keratoconic eyes, are located in the lower right part of the graphs; while eyes with small optical aberrations and large light scattering, such as cataractous eyes, are located in the upper left part of the graphs. Normal eyes are distributed in the lower left part, close to the origin.

The SPSS discriminant analysis correctly classified normal, keratoconic, and cataractous eyes: 84% correct for the contrast method and 78% for the PSF method. The results were similar, because we found a good correlation between the contrast and PSF methods (Fig. 9), although the result with the contrast method was slightly better than that with the PSF method. Observing Fig. 5c for the contrast method and Fig. 6c for the PSF method (both graphs were generated by SPSS), we found more linear separation with the contrast method than with the PSF method, in which the plots of cataractous eyes were slightly distorted.

In Figs. 5a, b and 6a, b, error bars (standard error) show the precision of the multiple measurements. When the light scattering was large, as for cataractous eyes, the corresponding standard error was also large. For normal and keratoconic eyes, the standard error was small. Multiple measurements (we measured each eye three times in this study) are needed for the average of the results to be sufficient to distinguish cataracts.

As we wrote in the first sentence of this paper, vision is affected by light scattering. Once we confirm the methods used to estimate forward light scattering of the crystalline lens by further studies, we may be able to elucidate the phase function in the light scattering of the lens. For now, by means of the Monte-Carlo method, retinal images degraded by light scattering suffice for estimating the phase function.[20]

Acknowledgments. The authors thank Prof. Howard C. Howland and Dr. Tong Li of Cornell University for their helpful comments on the manuscript.

References

1. Hess R, Woo G. Vision through cataracts. Invest Ophthalmol Vis Sci 1978;17:428–435.
2. IJspeertJK, de Waard PWT, van den Berg TJTP, de Jong PVTM. The intraocular straylight function in 129 healthy volunteers; dependence on angle, age and pigmentation. Vision Res 1990;30:699–707.
3. Liang J, Grimm B, Goelz S, Bille JF. Objective measurement of wave aberrations of the human eye with the use of a Hartmann-Shack wave-front sensor. J Opt Soc Am A Opt Image Sci Vis 1994;11:1949–1957.
4. Liang J, Williams DR. Aberrations and retinal image quality of the normal human eye. J Opt Soc Am A Opt Image Sci Vis 1997;14:2873–2883.
5. MacRae SM, Williams DR. Wavefront guided ablation. Am J Ophthalmol 2001;132:915–919.
6. Liang J, Williams DR, Miller DT. Supernormal vision and high-resolution retinal imaging through adaptive optics. J Opt Soc Am A Opt Image Sci Vis 1997;14:2884–2892.
7. Roorda A, Williams DR. The arrangement of the three cone classes in the living human eye. Nature 1999;397:520–522.
8. Maeda N, Fujikado T, Kuroda T, et al. Wavefront aberrations measured with Hartmann-Shack sensor in patients with keratoconus. Ophthalmology 2002;109:1996–2003.
9. Kuroda T, Fujikado T, Maeda N, Oshika T, Hirohara Y, Mihashi T. Wavefront analysis in eyes with nuclear or cortical cataract. Am J Ophthalmol 2002;134:1–9.
10. Kuroda T, Fujikado T, Maeda N, Oshika T, Hirohara Y, Mihashi T. Wavefront analysis of higher-order aberrations in patients with cataract. J Cataract Refract Surg 2002;28:438–444.
11. Koh S, Maeda N, Kuroda T, et al. Effect of tear film break-up on higher-order aberrations measured with wavefront sensor. Am J Ophthalmol 2002;134:115–117.
12. Montes-Mico R, Alio JL, Munoz G, Perez-Santonja JJ, Charman WN. Postblink changes in total and corneal ocular aberrations. Ophthalmology 2004;111:758–767.
13. Hockwin O, Dragomirescu V, Laser H. Measurements of lens transparency or its disturbances by densitometric image analysis of Scheimpflug photographs. Graefes Arch Clin Exp Ophthalmol 1982;219:255–262.
14. Chylack LT, Jr., Wolfe JK, Singer DM, et al. The Lens Opacities Classification System III. The Longitudinal Study of Cataract Study Group. Arch Ophthalmol 1993;111:831–836.
15. Liang J, Westheimer G. Optical performances of human eyes derived from double-pass measurements. J Opt Soc Am A Opt Image Sci Vis 1995;12:1411–1416.
16. Thibos LN, Hong X. Clinical applications of the Shack-Hartmann aberrometer. Optom Vis Sci 1999;76:817–825.
17. Donnelly WJ 3rd, Pesudovs K, Marsack JD, Sarver EJ, Applegate RA. Quantifying scatter in Shack-Hartmann images to evaluate nuclear cataract. J Refract Surg 2004;20:S515–522.
18. Kuroda T, Fujikado T, Ninomiya S, Maeda N, Hirohara Y, Mihashi T. Effect of aging on ocular light scatter and higher order aberrations. J Refract Surg 2002;18:S598–602.
19. Fujikado T, Kuroda T, Maeda N, et al. Light scattering and optical aberrations as objective parameters to predict visual deterioration in eyes with cataracts. J Cataract Refract Surg 2004;30:1198–1208.
20. Hair JF, Anderson RE, Tatham RL, Black WC. Multivariate data analysis. 5th ed. Upper Saddle River, NJ: Prentice Hall; 1998.
21. Jahns J, Walker SJ. Two-dimensional array of diffractive microlenses fabricated by thin film deposition. Appl Opt 1990;7:931–936.
22. Pierscionek B, Green RJ, Dolgobrodov SG. Retinal images seen through a cataractous lens modeled as a phase-aberrating screen. J Opt Soc Am A Opt Image Sci Vis 2002;19:1491–1500.
23. Born M, Wolf E. Principles of optics. 6th ed. Oxford: Pergamon; 1980.
24. Artal P, Iglesias I, Lopez-Gil N, Green DG. Double-pass measurements of the retinal-image quality with unequal entrance and exit

pupil sizes and the reversibility of the eye's optical system. J Opt Soc Am A Opt Image Sci Vis 1995;12:2358–2366.
25. Diaz-Santana L, Dainty JC. Effects of retinal scattering in the ocular double-pass process. J Opt Soc Am A Opt Image Sci Vis 2001;18:1437–1444.
26. Bohren CF, Huffman DR. Absorption and scattering of light by small particles. New York: Wiley; 1983.
27. Laven P. MiePlot. http://www.philiplaven.com/mieplot.htm.
28. van den Berg TJ, Spekreijse H. Near infrared light absorption in the human eye media. Vision Res 1997;37:249–253.
29. Gilliland KO, Freel CD, Johnsen S, Craig Fowler W, Costello MJ. Distribution, spherical structure and predicted Mie scattering of multilamellar bodies in human age-related nuclear cataracts. Exp Eye Res 2004;79:563–576.
30. Tuchin V. Tissue optics: light scattering methods and instruments for medical diagnosis. Bellingham, Washington: SPIE Press; 2000.
31. Cox MJ, Atchison DA, Scott DH. Scatter and its implications for the measurement of optical image quality in human eyes. Optom Vis Sci 2003;80:58–68.
32. van den Berg TJ, Spekreijse H. Light scattering model for donor lenses as a function of depth. Vision Res 1999;39:1437–1445.
33. van de Hulst HC. Light scattering by small particles. New York: Wiley; 1957.

Wavefront Analysis of Eye With Monocular Diplopia and Cortical Cataract

Takashi Fujikado, MD, Hiroshi Shimojyo, MD, Jun Hosohata, MD, Yoko Hirohara, BS, Toshifumi Mihashi, BE, Naoyuki Maeda, MD, and Yasuo Tano, MD

PURPOSE: To determine whether higher-order aberrations can explain the monocular diplopia reported by a patient.

DESIGN: Observational case report.

METHODS: A patient complaining of monocular diplopia was examined with the Hartmann-Shack aberrometer to determine if the higher-order wavefront aberrations could account for the diplopia. The patient had a mild cortical cataract, and measurements were made before and after lensectomy. In addition, the retinal image was simulated using Zernike polynomials.

RESULTS: Spherical aberration (0.20 μm for 4-mm pupil) and secondary astigmatism (−0.12 μm) were increased in the eye. The simulated retinal image had a double configuration that was approximately the same as the subjective image reported by the patient. After cataract surgery, the diplopia disappeared, and the spherical aberrations and secondary astigmatism were considerably decreased.

CONCLUSIONS: The monocular diplopia probably stemmed from the combined effects of spherical aberration and secondary astigmatism caused by the cortical cataract. (Am J Ophthalmol 2006;141:1138–1140. © 2006 by Elsevier Inc. All rights reserved.)

OPTICAL IRREGULARITIES IN THE EYE ARE REPORTED to cause monocular polyopia.[1–3] Monocular triplopia in eyes with nuclear cataracts were reported to be caused by a combination of trefoil and spherical aberrations.[4] Although it is known that astigmatism combined with spherical errors can cause monocular diplopia, whether the monocular diplopia can be due to ocular higher-order aberrations has not been well investigated. We present a patient who complained of monocular diplopia and was examined with the Hartmann-Shack aberrometer to determine whether the higher-order aberrations could account for the diplopia.

A 44-year-old man complained of monocular diplopia in his right eye of two years' duration. On the first visit, his best-corrected visual acuity was 20/25 in his right eye, and the subjective refraction was S 1.75 diopters = C −1.25 diopters Ax 60 degree. Slit-lamp examination revealed a mild cortical cataract in the right eye (Figure 1).

Hartmann-Shack aberrometer (Wavefront analyzer, KR9000PW, Topcon Corp, Tokyo, Japan)[5] measurements showed a marked increase in the root mean square value of the ocular secondary astigmatism (C_4^{-2}, −0.12 μm) and spherical aberration (C_4^{0}, 0.20 μm). For the cornea, C_4^{-2} was −0.01 μm and C_4^{0} was 0.05 μm. A color-coded map of higher-order aberration showed almost normal pattern in the cornea but delayed wavefront in the periphery and advancement of wavefront in the center in oculus (Figure 2). These data indicate that the positive spherical aberration combined with a secondary astigmatism was increased in the internal optics, mainly in the crystalline lens.

The simulated retinal image of a Landolt C using the data of Zernike polynomials showed a double configuration

AJO.com Supplemental Material available at AJO.com.

Accepted for publication Dec 29, 2005.

From the Departments of Applied Visual Science (T.F.) and Ophthalmology (H.S., J.H., N.M., Y.T.), Osaka University Graduate School of Medicine, Technical Research Institute, and Topcon Corporation (Y.H., T.M.), Tokyo, Japan.

Supported in part by Health Science Research Grants from the Ministry of Health, Labor and Welfare, Japan, and by grant 16591752 from the Ministry of Education, Culture, Science and Technology.

Inquiries to Takashi Fujikado, MD, Department of Applied Visual Science, Osaka University Graduate School of Medicine, 2-2 Yamadaoka, Suita-shi Osaka, 565-0871, Japan; e-mail: fujikado@ophthal.med.osaka-u.ac.jp

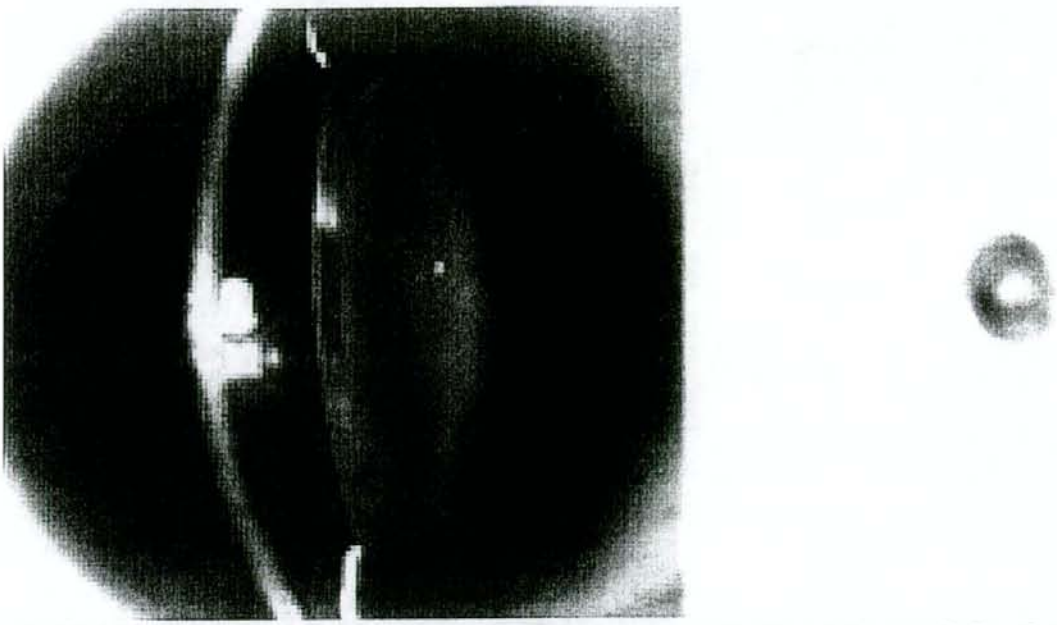

FIGURE 1. Monocular diplopia and cortical cataract. Slit-lamp photography reveals mild cortical cataract (Left), and simulated image for Landolt C from ocular higher-order aberration shows double configuration (Right).

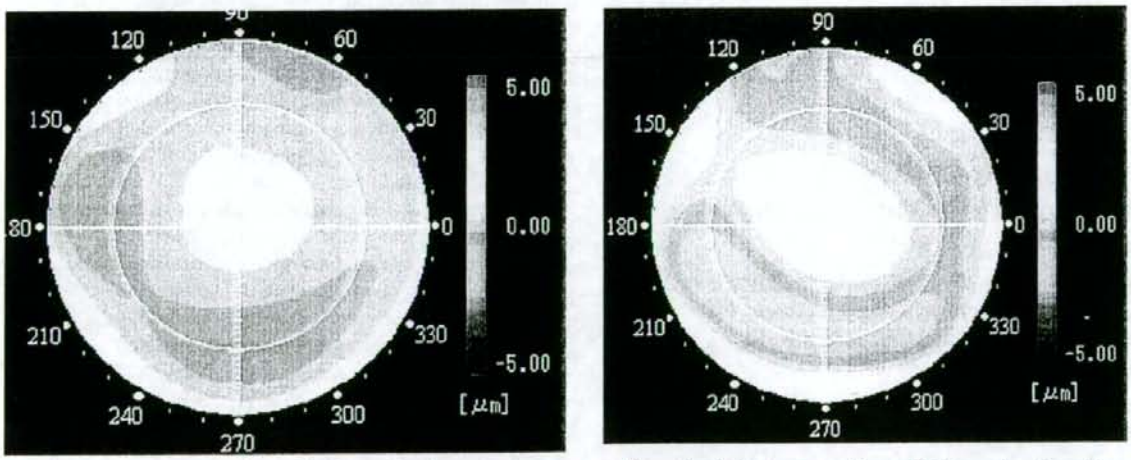

FIGURE 2. Wavefront analysis of higher-order aberration in cornea and in oculus before surgery. Corneal higher-order aberrations have almost normal pattern (Left), but ocular higher-order aberrations show advancement of wavefront (warm color) in central pupillary area and delay of wavefront (cool color) in peripheral pupillary area (Right).

(Figure 1), which was very similar to the subjective image described by the patient.

After explaining that his monocular diplopia probably originated from the cataract and the risks and benefits of the surgery, informed consent was obtained for lensectomy.

After cataract surgery, his best-corrected visual acuity improved to 20/13, and both the secondary astigmatism and spherical aberration were markedly decreased (C_4^{-2}, 0.01 μm, C_4^{0}, 0.09 μm for 4-mm pupil). The diplopia disappeared, and the simulated retinal image was normal (Figure 3).

Measurements with the H-S aberrometer have shown that not only light scattering but also higher-order aberrations lead to a deterioration of the retinal image.[5] In our patient,

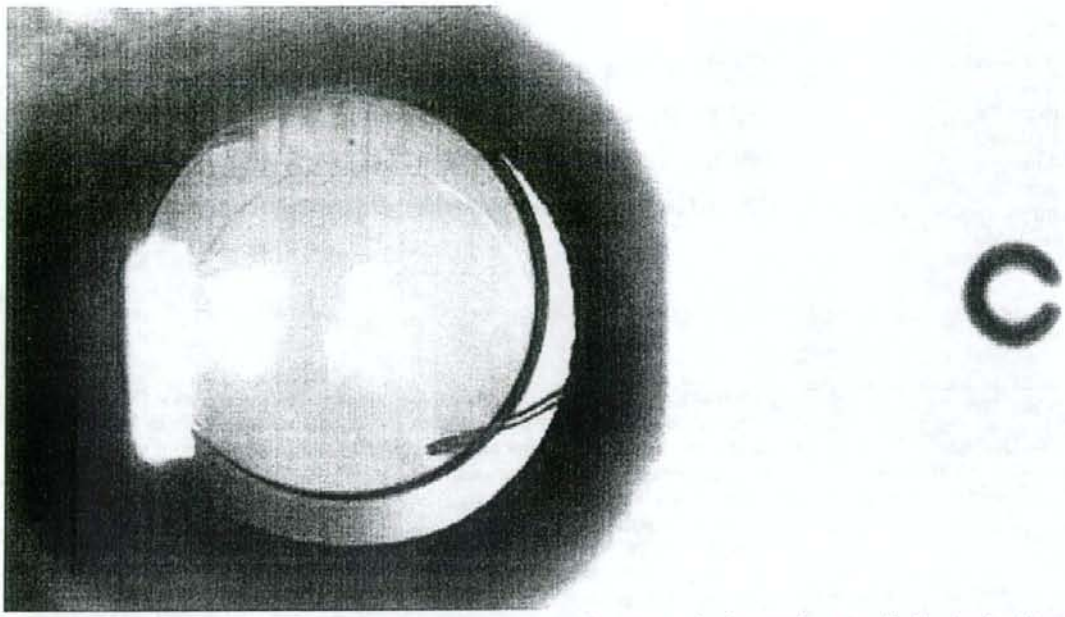

FIGURE 3. Disappearance of monocular diplopia after surgery. After intraocular lens implantation (Left), simulated image for Landolt C from ocular higher-order aberration showed normal pattern (Right).

the secondary astigmatism and spherical aberration were greatly increased, and the simulated retinal image had a double configuration. This image corresponded with the subjective diplopia (Figure 1).

The double configuration of the retinal image was determined to originate from the cortical cataract because the higher-order aberrations of the cornea were different from that of the oculus (Figure 2), and because the diplopia disappeared after lensectomy.

The increase of positive spherical aberration was due to the development of the cortical cataract,[5] and the increase of secondary astigmatism might be related to the effect of spokelike irregularities in the lens. To our knowledge, this is the first report that has demonstrated a relationship between ocular higher-order aberrations and monocular diplopia.

REFERENCES

1. Fincham EF. Monocular diplopia. Br J Ophthalmol 1963;47: 705–712.
2. Bour L, Apkarian P. Segmented refraction of the crystalline lens as a prerequisite for the occurrence of monocular polyopia, increased depth of focus, and contrast sensitivity function notches. J Opt Soc Am (A) 1994;11:2769–2276.
3. Kluxen G. Die polyopia monocularis bei kernkataract. Klin Mbl Augenheilk 1985;187:270–272.
4. Fujikado T, Kuroda T, Maeda N, et al. Wavefront analysis of monocular triplopia in the eye of nuclear cataract. Am J Ophthalmol 2004;137:361–363.
5. Kuroda T, Fujikado T, Maeda N, Oshika T, Hirohara Y, Mihashi T. Wavefront analysis in eyes with nuclear or cortical cataract. Am J Ophthalmol 2002;134:1–9.

Graefe's Arch Clin Exp Ophthalmol
(2006) 244: 1283–1292

CLINICAL INVESTIGATION

DOI 10.1007/s00417-006-0260-3

Takeshi Morimoto
Takehiro Fukui
Kenji Matsushita
Yoshitaka Okawa
Hiroshi Shimojyo
Shunji Kusaka
Yasuo Tano
Takashi Fujikado

Evaluation of residual retinal function by pupillary constrictions and phosphenes using transcorneal electrical stimulation in patients with retinal degeneration

Received: 23 July 2005
Revised: 12 December 2005
Accepted: 3 January 2006
Published online: 21 March 2006

This study was supported by Health Science Research Grants from the Ministry of Health, Labor and Welfare, Japan and by a grant from the Ministry of Education, Culture, Science and Technology (no.16591752). T. Morimoto was supported by the JSPS Research Fellowship for Young Scientists.

T. Morimoto · T. Fukui · Y. Okawa · S. Kusaka · T. Fujikado (✉)
Department of Applied Visual Science, Osaka University Graduate School of Medicine,
2-2 Yamadaoka, Suita,
Osaka, 565-0871, Japan
e-mail: fujikado@ophthal.med.osaka-u.ac.jp
Fax: +81-6-68793458

K. Matsushita · H. Shimojyo · Y. Tano
Department of Ophthalmology, Osaka University Graduate School of Medicine,
2-2 Yamadaoka, Suita,
Osaka, 565-0871, Japan

Abstract *Background:* To evaluate inner-retinal function by pupillary constrictions and phosphenes evoked by transcorneal electrical stimulation (TES) in patients with hereditary retinal degeneration. *Methods:* Consecutive 20 eyes of 20 patients (16 with retinitis pigmentosa (RP); and four with cone-rod dystrophy (CRD)) whose visual acuity was equal to or worse than 20/2000 at Osaka University Hospital and eight eyes of eight healthy subjects were enrolled. TES was performed on with a contact lens stimulating electrode. The electrically evoked pupillary response (EEPR) was recorded by a pupillometer, and the phosphenes by the subjective responses. Three electrical current thresholds were determined: T1, threshold current for initial phosphene; T2, threshold for eliciting a phosphene extending into the central field; and P, threshold for a relative pupillary constriction ≥3%. The EEPR and phosphene thresholds were compared with the visual acuity or the visual field. *Results:* All T1, T2 and P were significantly higher in patients than in normals (Mann-Whitney, $P<0.001$). Both T1 and T2 were not correlated with visual acuity but depended on the area and location of the residual visual field. T1 and T2 in RP eyes with a EEPR was significantly lower than that in RP eyes without an EEPR. During TES, all subjects and patients had no pain, and no complications except for a slight corneal superficial punctuate keratopathy. *Conclusions:* The safety and the efficacy of TES to estimate the residual inner-retinal function in patients with retinal degeneration indicate that TES can be used as one of the most important test to select candidates for retinal prostheses.

Keywords Retinitis pigmentosa · Cone-rod dystrophy · Pupillary reflex · Phosphene · Transcorneal electrical stimulation

Introduction

Retinitis pigmentosa (RP) is one of the leading causes of blindness in the world. RP includes a group of heredity retinal degenerations that primarily affects photoreceptor (PR) function [18, 23]. In the last stage of the disease, RP patients have little or no functional vision.

To restore some vision to patients with RP, the strategy of replacing the degenerated photoreceptors by a bionic device called a "retinal prosthesis" is under serious study [17, 36]. Various types of retinal prosthesis have been proposed and tested in animals [2, 8, 11, 13, 16, 28, 34] and patients [3, 10, 26, 33]. A typical retinal prosthesis consists of an array of electrodes that is implanted on the retinal surface and is used to deliver electrical current to the retina to evoke a light sensation called a phosphene.

Another approach to restore vision in RP patient is to transplant retinal progenitor cells (RPCs) into the retina [7, 36]. The success of an artificial retina or the transplantation of RPCs to restore vision depends on the presence of

physiologically intact retinal ganglion cells (RGCs) which can transmit visual signals to the brain.

Morphometric studies of the retinas in RP patients have shown the preservation of some of the RGCs [9, 27, 29]. Postmortem studies of RP eyes have shown that the number of RGC was approximately 30% of that in normal age-matched eyes in the macular area but only 20% in extramacular regions [9, 27]. On the other hand, it must be remembered that remodeling and ectopic retinal structures develop in RP retinas [5, 15]. Retinal remodeling and retinal circuit corruption may prevent the surviving RGCs from transmitting visual signals.

Given these pieces of evidence, a small number of RGCs are certainly present in the eyes of RP patients. However, it is difficult to determine to what extent these RGCs are functional compared with those in an intact retina because the method to evaluate the residual RGC function is limited.

Electroretinography (ERG) and visually evoked potentials (VEPs) are of little value when only a small number of PRs remain in the degenerated retina. On the other hand, electrical stimulation to evoke phosphenes is a potential useful method to evaluate the function of residual RGCs in humans. Phosphenes generated by galvanic or faradaic currents passed through the orbit by various electrode arrangements have been reported since the mid-20th century [1, 6, 19, 20]. More recent studies have used transcorneal electrical stimulation (TES) using corneal electrodes under local anesthesia to evoke phosphenes and to obtain electrically evoked responses (EER) in healthy subjects [21, 24] and RP patients [22, 25].

Although it is not conclusive what kind of retinal neurons are primarily stimulated by TES, the RGCs must be finally activated to transmit visual signals to the brain when a phosphene is evoked. Thus, TES could be one way to estimate the function of the residual RGCs in patients.

The area of the perceived phosphene may correspond to the area where functional RGCs are present and the extent of residual inner retinal function in a degenerated retina. However, it is difficult to assess the RGC function based on the evaluation of phosphene, because phosphene is a subjective sensation. Delbeke et al. tried to compare the phosphenes to somatosensory sensation or pain of the eyelid evoked by electrical stimulation through the eyelid to assess the function of RGCs in patients [4]. Because the somatosensory sensation is also a subjective parameter and is not directly related to phosphenes, the assessment of RGC function based on the somatosensory sensation is limited for candidates of retinal prosthesis [3, 10, 26], even though it is effective for candidates of optic nerve stimulation [33].

Direct and indirect pupillary constrictions can be evoked by TES by stimulating the afferent pupillary pathway and are called electrically evoked pupillary responses (EEPR) [30, 31]. The EEPR can be an objective parameter to be compared with phosphene; however, the relationship between phosphenes and EEPR has not been determined.

Thus, the purpose of this study was to investigate the phosphenes and EEPR in healthy subjects and in patients with retinal degeneration, and to compare these findings to the visual function in these eyes. The long term goal of our studies is to develop a simple and safe method to evaluate the function of the residual RGCs by combining phosphenes and EEPR to select candidates for the retinal prosthesis implant.

Materials and methods

Setting These studies were performed at the Osaka University Medical School, Osaka, Japan.

Patients The characteristics of all subjects are shown in Tables 1 and 2. Eight eyes of eight male volunteers (34±6 years, mean age±SD) with no ocular disorders, and consecutive 20 eyes of 20 patients (51±13 years) with hereditary retinal degeneration [16 patients had RP and four patients had cone-rod dystrophy (CRD)] who visited Osaka University Hospital between January 2003 and December 2003 were studied. The diagnosis was confirmed by independent ophthalmologic and ERG examinations. The inclusion criteria for patients was that the visual acuity was equal or lower than 20/2000, which was lower than the intended resolution of our project of artificial retina. The exclusion criteria were those patients with cardiac pacemaker or the presence of corneal diseases.

All subjects gave an informed consent after the purpose of this study and the procedures to be used were explained. They were free to withdraw at any time. This study adhered to the Declaration of Helsinki and was approved by the Ethics Committee of Osaka University Hospital.

The slit-lamp examination of the corneal was performed just after the TES examination in all subjects.

Table 1 Characteristics of normal subjects

No	Age	Sex	T1 (μA)	T2 (μA)	P (μA)
1	49	M	75	100	125
2	34	M	50	100	125
3	27	M	50	75	125
4	32	M	75	125	150
5	31	M	75	125	150
6	32	M	75	125	150
7	32	M	100	150	200
8	33	M	25	75	75

T1 threshold current of initial perceptual phosphene; *T2* threshold current of phosphene expanding over the center of visual field; *P* threshold current of EEPR

Table 2 Characteristic of patients

No	Age	Sex	VA	T1 (μA)	T2 (μA)	P (μA)	RPC (%)	CVF (deg^2)	PVF (deg^2)	Diagnosis
1	60	F	HM	200	250	600	N	0	1.5×10^3	CRD
2	9	M	20/2000	200	250	250	13	0	1.9×10^4	CRD
3	31	M	20/2000	50	600	600	N	0	7.9×10^3	CRD
4	32	F	20/2000	200	700	300	15	0	1.4×10^4	CRD
5	42	F	20/2000	550	550	N	5.2	1.7×10^2	3.0×10^3	RP
6	51	F	NLP	650	650	NR	NR	0	0	RP
7	50	F	NLP	150	550	NR	NR	0	0	RP
8	23	M	CF	400	400	400	N	0	2.8×10^3	RP
9	45	F	HM	300	350	550	N	3.4×10	0	RP
10	66	F	20/2000	550	700	800	8	4.6×10^2	0	RP
11	44	F	20/2000	600	600	NR	NR	2.9×10	0	RP
12	50	M	20/2000	150	150	600	N	2.5×10	0	RP
13	56	M	HM	550	700	N	2.1	4.1×10	0	RP
14	55	M	HM	1,500	1500	N	4.6	6.1×10	0	RP
15	56	F	20/2000	500	500	1500	7.6	2.0×10^2	0	RP
16	62	F	HM	500	500	900	N	3.4×10	0	RP
17	65	M	LP	1,000	1400	N	N	0	0	RP
18	66	M	LP	1,100	N	N	N	0	0	RP
19	62	F	20/2000	350	700	N	N	2.4×10^2	0	RP
20	66	M	LP	1,400	1400	N	N	0	0	RP

F female, *M* male, *VA* visual acuity; *NLP* no light perception; *HM* hand motion; *CF* counting fingers; *LP* light perception; *T1* threshold current of initial perceptual phosphene; *T2* threshold current of phosphene expanding over the center of visual field; *P* threshold current of EEPR; *RPC* relative pupillary constriction by flash-light stimulation measured by pupillography; *N* not responded; *NR* non-recordable due to nystagmus; *CVF* area of preserved central visual field within a radius of 30°; *PVF* area of peripheral visual field left outside the radius of 30°; *CRD* cone rod dystrophy; *RP* retinitis pigmentosa

Assessment of visual function

The best-corrected visual acuity was measured by a certified orthoptists with a standardized Landolt visual acuity chart. The visual field was quantitatively determined by kinetic perimetry using a Goldmann perimeter. The V/4e target with a luminance of 320 cd/m^2 was projected on a background with a luminance of 10 cd/m^2. The area of the visual fields was calculated using the Scion Image program (Scion Corporation, Frederick, Mass., USA).

Transcorneal electrical stimulation

TES was performed on eight healthy subjects and 20 patients. Before the TES, the cornea was anesthetized with 0.4% oxyburocaine hydrochloride, and the cornea was covered with 3% hyaluronic acid and 4% chondroitin sulfate (Viscoat, Alcon Japan Ltd, Tokyo, Japan) to protect it from injury by the contact lens electrode. A concentric bipolar contact lens electrode (Burian-Allen; Hansen Ophthalmic Laboratories, Iowa City, Iowa, USA) was placed on the cornea, and electric current pulses (20 pulses) were delivered from a stimulator SEN-7203 (Nihonkoden, Tokyo, Japan) and stimulus isolator unit A395 (WPI, Sarasota, Fla., USA) through the two electrodes embedded in the contact lens.

The electrical stimuli were rectangular, biphasic (anodic first) pulses of 10 ms/phase duration, frequency with 20 Hz, and train of 20 paired pulses. These parameters were chosen based on the psychophysical experiment on normal volunteers to elicit phophesene effectively (Matsushita K et al., ARVO abstract 2003). The current intensity ranged from 50 μA to 2 mA with a step of 25 μA up to 100 μA, 50 μA up to 1000 μA, and 100 μA above 1000 μA.

Recording the pupillary constriction

An infrared pupillometer, the IRISCORDER C7364 (Hamamatsu, Hamamatsu, Japan), was used to measure the pupillary responses evoked by TES. The pupillometer is equipped with an infrared charge-coupled device (CCD) camera and recorded the pupillary diameters at a 60 Hz sampling rate. Normal subjects and patients wore a goggle equipped with the CCD camera and the red light-emitting diode (LED) stimulus light (660 nm; maximum light power of 10±3 μW; stimulus duration of 0.1 s). Before inserting the contact lens electrode, the direct and consensual pupillary light reflex of normal subjects and patients were recorded. After inserting the contact lens electrode,

the EEPRs were recorded from the fellow eye. The relative amplitude of the pupillary constriction was determined by calculating the relative amplitude of pupillary constriction starting from the baseline diameter at the stimulus onset to the peak of the pupillary constriction as follows:

$$Relativepupillaryconstruction(RPC\%) = 100(a-b)/a$$

where a=pre-stimulus baseline pupil size (mm), and b=maximally constricted pupil size (mm).

The threshold current for a relative pupillary constriction was determined by the minimal electrical current necessary to elicit an EEPR of ≥3 %.

Psychophysical procedures

We recorded the characteristics of the phosphenes (e.g. location, size, color, brightness, shape) for each electrical current intensity in the dark room. Subjects were masked to the test conditions, as this allowed each subject to provide a non-biased descriptions of their perception. The examiner, who was aware of the stimulus conditions, asked questions about the phosphene. False positive trials (i.e. no stimulus presented) were included to determine the reliability of the responses.

Two thresholds were determined; threshold 1 (T1) was defined as the value of the electrical current that elicited the first perceived phosphene anywhere in the visual field, and threshold 2 (T2) was the value at which the subjects perceived a phosphene extending into the center of the visual field. We determined the two thresholds by starting with a current intensity below threshold and increasing the stimulus strength stepwise until a perception of a phosphene was first perceived (T1a), and the current at which the phosphene extended into the central visual field (T2a). Next, the stimulus strength was started well above threshold and reduced along the same steps until the same perceptions were obtained, i.e. disappearance of the phosphene from the central visual field (T2b), and the complete disappearance of a phosphene (T1b). T1a and T1b are usually the same but if the values differed, we averaged the two values to determine the threshold (T1). The same procedure was taken to determine the value of T2. For each step, the patient was asked to describe his/her perceptions in detail which were recorded on audio tape.

Statistical analyses

Data are presented as the means±standard error of the means (SEM), and statistically analyzed with the SPSS 10.0J program (SPSS Inc, Chicago, Ill., USA). Comparisons between two groups were made by the student *t*-test when data were normally distributed, or by the Mann-Whitney *U*-test when data were not normally distributed. The degree of correlation was evaluated by the coefficient of correlation (r) calculated using Pearson correlation coefficient. Comparisons between the three groups were made by one-way ANOVA followed by the Tukey test when data were normally distributed. The probability level is represented as the value "*P*"; statistical significance was set at $P<0.05$.

Results

Characteristics of phosphenes in normal subjects and patients

In normal subject, phophene was first perceived in the upper or lower peripheral field with the mean threshold of 65±8 μA (T1). With a further increase in the current intensity, phosphene spread into the center of the visual field with the mean threshold of 109±9 μA (T2). With a further increase in the current intensity, a pupillary constriction was evoked with a mean intensity to evoke a RPC of just >3% was 138±13 μA (P). A comparison of the three thresholds, T1, T2, and P, showed that they were significantly different from each other ($P<0.001$, one-way ANOVA) (Table 1, Fig. 1).

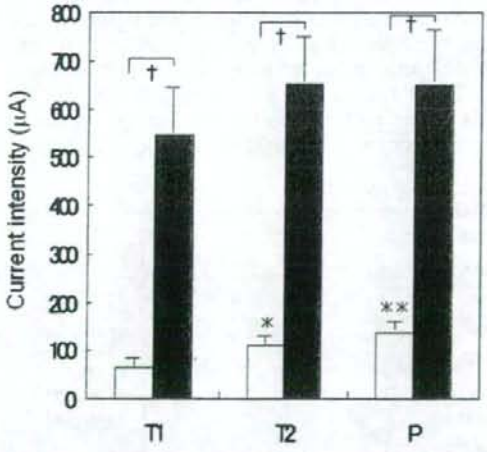

Fig. 1 Average threshold current intensities of phosphenes and pupillary constrictions in normals (*open bar*) and in eyes with retinal degeneration (*filled bar*). *T1* threshold current intensity of initial phosphene, *T2* threshold current intensity for phosphene covering the center of visual field, *P* threshold current intensity of electrically evoked pupillary response (*EEPR*) . Data are presented as mean± SEM. There was a significant difference among three thresholds in normals (one-way ANOVA, $P< 0.01$; Tukey test, * $P<0.05$, ** $P<0.01$, vs T1). No significant difference among three thresholds was obtained in eyes with retinal degeneration. There was a significant difference in each threshold between normals and retinal degeneration (Mann-Whitney Rank Sum Test,† $P<0.001$)

The distribution of the T1, T2, and P thresholds in patients are shown in Table 2. A phosphene was elicited by TES in all patients. However, the threshold currents were much higher than normal subjects and varied considerably among patients. The mean T1 threshold was 545±411 μA. With an increase in the current intensity, many patients reported that bright light sensation spread toward the center of visual field. The mean T2 threshold was 723±479 μA. However patient 18, mentioned that the phosphene did not spread into the center with maximum current intensities (2000 μA). The threshold of P was higher than T2 in most cases but in some patients, pupillary reflex was not evoked with the maximum current intensities (2000 μA) (Table 2, Fig. 1). The false positive rate was 0% in the subjective phosphene test.

Relationship between thresholds (T1 and T2) in patients and normal subjects

Although the thresholds of the normal subjects were quite comparable, the thresholds of the patients varied considerably. A scatter plot of T2 as a function of T1 in normal subjects and patients is shown in Fig. 2. In the normal subjects, a highly significant positive correlation was observed between the T1s and T2s (r=0.900 and P=0.002; Pearson's correlation coefficient).

The patients, on the other hand, were divided into two groups from the scatter plot. One group was made up of patients whose thresholds were distributed tightly around the linear regression line of normal subjects, and the thresholds of other group of patients were shifted above the line. These results lead us to examine whether the thresholds in the patients were dependent on the visual acuity or the residual visual field or the type of disease.

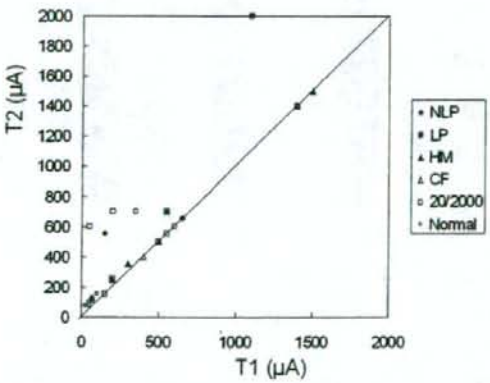

Fig. 2 Comparison of T1 with T2 in normal subjects and patients. Normal subjects (*open circles*) and patients (*filled circles*) are plotted. Patients were divided into two groups. One group includes patients with a closer fit to the linear regression line of normal subjects, another group included patients distributed above the line

Relationship between thresholds and visual acuities in patients

The visual acuities were converted to the logarithm of the minimum angle of resolution (logMAR) units for the statistical analysis. For visual acuities less than 20/2,000 (2.0 logMAR units), the following log MAR values were assigned [12]: 2.6 logMAR for counting finger (CF); 2.9 logMAR for hand motion (HM), 3.1 logMAR for light perception (LP); and 3.4 logMAR for no light perception (NLP). The relationship between the electrical phosphene thresholds and logMAR visual acuities is shown in Fig. 3. There was no significant relationship (T1,r=0.433; P=0.056: T2,r=0.417; P=0.067) between log MAR visual acuities and thresholds (Fig. 3a,b). For example, although patients 6 and 7 were NLP, their thresholds were lower than those of 11 and 14, whose visual acuities were 20/2000 and HM, respectively (Table 2).

Relationship between thresholds of phosphenes and residual visual fields in patients

The patients were classified into three groups on the basis of the location of residual visual field: type C, visual field present within the central 30° radius (n=10); type P, peripheral visual field left beyond the central 30° radius (n=5); and type N, complete loss of visual field (n=5). A patient who had two islands of visual field with one located within 30° radius was categorized as type C.

The relationship between the thresholds and type of residual visual fields is shown in Fig. 4. There was a significant difference in the thresholds for a phosphene in the three groups (one-way ANOVA, T1, T2; P<0.05). The mean current intensities of T1 and T2 for type P patients were the lowest among the three groups: T1=210±56 μA; T2=440±91 μA, and for type C: (T1; 555±114 μA, T2; 625± 112 μA), and the mean intensities in type N were much higher (T1; 860±214 μA, T2; 1200±269 μA) (Fig. 4).

We further analyzed the relationship between the area of residual visual field and thresholds in each groups, and no significant correlation was found.

Relationship between thresholds of phosphenes and type of disease

In eyes with CRD, the cones are predominantly damaged and the loss of cones result in a loss of the central visual field, while in RP, the rods are predominantly damaged and the loss of rods result in a loss of the peripheral visual field. We therefore divided eyes with retinal degeneration into the CRD group and RP group (Fig. 5, Table 2).

The mean current intensity of T1 in the RP patients was significantly higher than that in CRD patients (640± 101 μA vs 163±38 μA, P<0.05; Fig. 5e). Although the

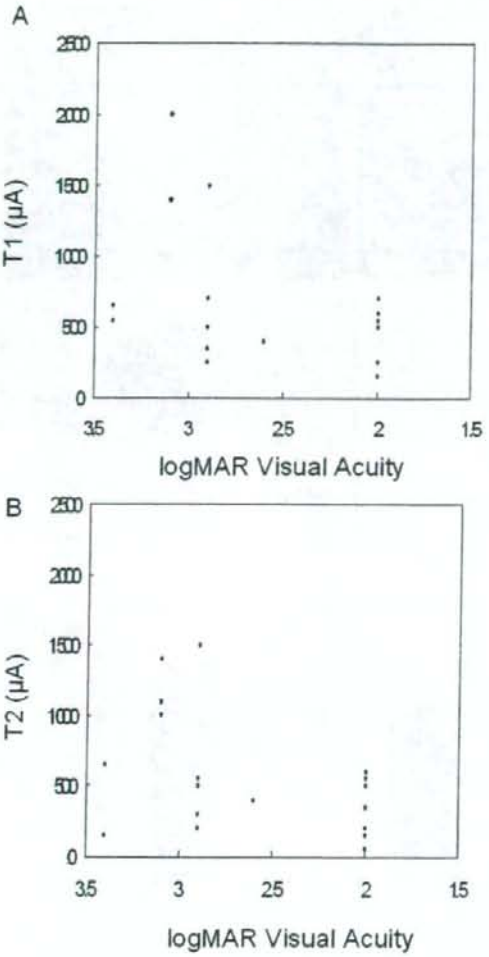

Fig. 3 Relationship between T1 and T2 and logMAR visual acuities in patients. **a**. T1s are plotted versus logMAR visual acuities, **b**. T2s are plotted versus logMAR visual acuities. There was no significant correlation between thresholds and logMAR visual acuities

mean current intensity of T2 in the RP patients was higher than in the CRD patients, the difference was not significant (790±126 μA vs 440±91 μA).

Relationship between pupillary responses and thresholds in RP patients

An EEPR was examined in all but three RP patients. These three had nystagmus and the tests for an EEPR could not be performed, and they were excluded from the analysis. An EEPR was recorded from all eyes with CRD, but 54%

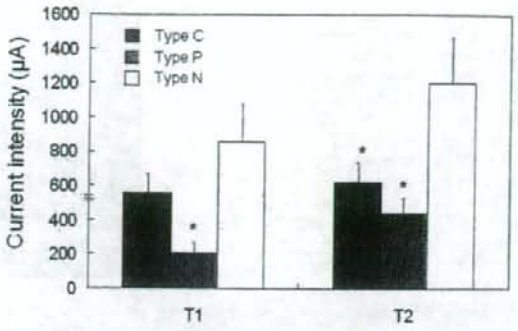

Fig. 4 Comparison of the type of residual visual fields with thresholds of phosphene. Type C; central visual field preserved within a 30° radius; type P, peripheral visual field left outside the central 30°; type N; complete loss of visual field. Data were presented as mean±SEM. There was a significant difference between three thresholds (one-way ANOVA: T1, T2; $P<0.05$; Tukey test, * $P<0.05$ vs type N)

(7/13) of the RP eyes did not show a positive EEPR (Fig. 6a).

The RP patients were classified into four groups on the basis of the presence or absence of a light and electrically-elicited pupillary response: type I, 15% (2/13) had light reflex (+) and EEPR (+); type II, 31% (4/13) had no light reflex (−) and had an EEPR (+); type III, 23% (3/13) had light reflex (+) and no EEPR (−); and type IV, 31% (4/13) had no light reflex (−) and no EEPR (−).

The waveform of the EEPR was very similar to that of the light response (Fig. 6a).

We examined the relationship between EEPR and thresholds of phosphenes in RP patients. We compared the thresholds of RP eyes that had a EEPR to those who did not have a EEPR. The absence or presence of EEPR completely divided patients into high or low thresholds groups. In the group with an EEPR, the mean current intensity of T1 was 400±62 μA, and the mean intensity of T2 was 433±75 μA. On the other hand, in the group without an EEPR, the mean intensities of T1 and T2 were significantly increased to 921±169 μA and 1,179±203 μA, respectively (T1, $P<0.05$; T2, $P<0.01$; Fig. 6b).

Side effects of TES examination

During the TES examination, no subjects complained pain or irritable sensation on cornea or upper lid. The slit-lamp examination after TES examination revealed a slight superficial punctuate keratopathy in all cases, which was comparable to those observed after the routine examination of electro-retinography.

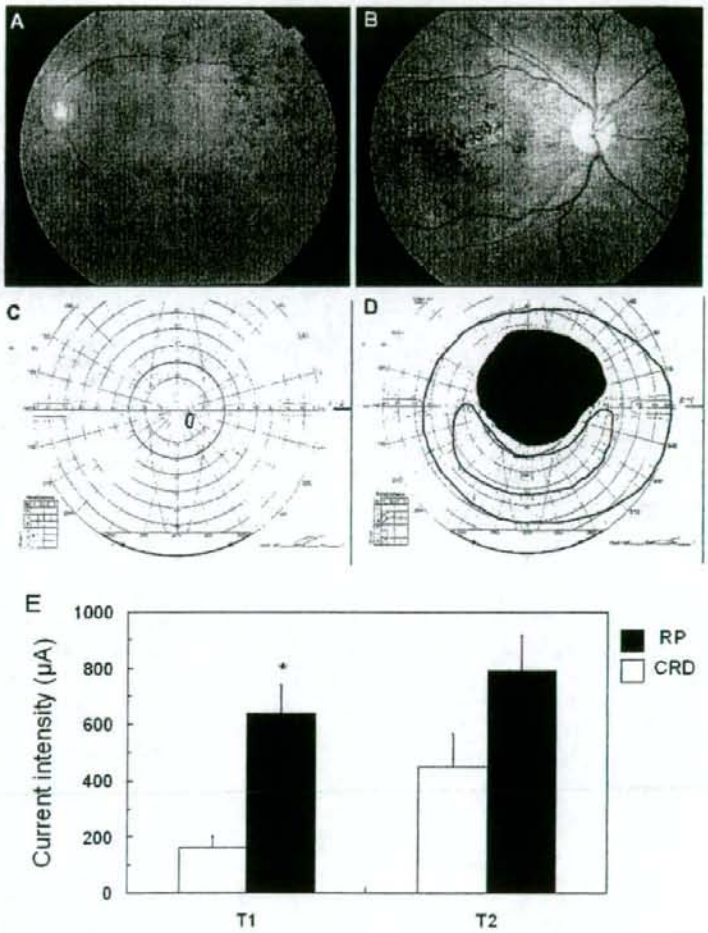

Fig. 5 Comparison of mean thresholds of RP patients with those of CRD patients. Representative fundus photographs and visual fields from two types of patients; **a** and **c** from a RP patient, **b** and **d** from a CRD patients. **e**. Mean thresholds of phosphene in two types of patients. There was a significant difference of T1 between the two groups (*, Mann-Whitney *U*-test, $P<0.05$); however, there was no significant difference in T2 between them

Discussion

Except a slight superficial punctuate keratopathy, no side effect was observed during or after TES, indicating that TES is a safe examination when performed along with our protocol.

The computer simulation showed that the charge density in the peripheral retina was higher than in the central retina if an eye was stimulated by a concentric corneal electrode [14], which was consistent with the observation that T2 was larger than T1. In order to elicit EEPR, more current was needed, suggesting that a more number of RGS should be involved to elicit pupillary reflex than to perceive phophene (Fig. 1).

A possibility that a direct current affected the pupil efferent and elicited the EEPR was neglected by the report that in eyes of optic atrophy, EEPR was not induced in the contra lateral healthy eye [32].

All RP patients perceived a phosphene, but the average threshold current of T1 or T2 was 7–8 times greater in RP patients than in normal subjects, suggesting that the number of residual RGC was much smaller in RP patients than in normal subjects [9, 27]. (Fig. 1). The threshold current of phosphenes varied among the patients, indicated that the residual RGCs function varied among patients (Table 2).

A plot of T1 and T2 in normal subjects and patients showed two groups. In one group, T2 was highly correlated with T1 as in normal subjects, and in the other group, the T2 was elevated relative to T1 (Fig. 2). These results indicate that in the former group, the rate of RGC loss in macula area may be similar to that in the extramacular area as reported [9, 27, 29], while in the latter group, the degree of RGC loss in the macula may be higher than that in the extramacular area.

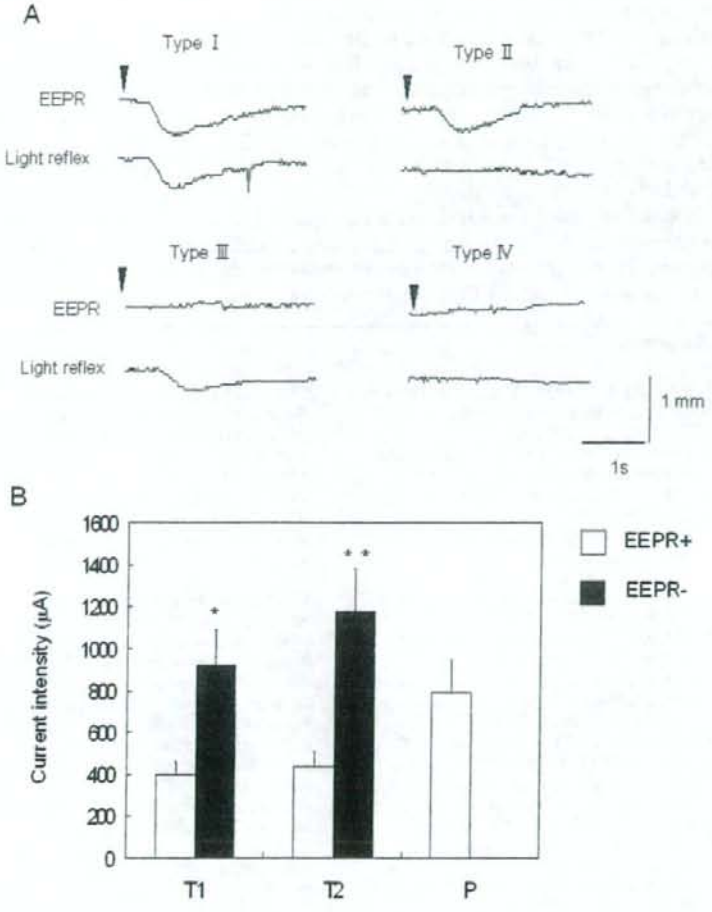

Fig. 6 **a**. Four types recordings of EEPR and light reflex from RP patients. Type I light reflex (+) and EEPR (+), type II light reflex (−) and EEPR (+), type III light reflex (+) and EEPR (−), and type IV light reflex (−) and EEPR (−). *Arrow head* indicates the onset of stimulation. **b**. Comparison of thresholds in RP patients with an EEPR (type I and type II) with RP patients without an EEPR (type III and type IV) There were significant differences between patients with an EEPR and without an EEPR (student *t*-test: T1; **P*<0.05, T2; ***P*<0.01)

We also found that the threshold of phosphenes and logMAR visual acuity were not significantly correlated. The thresholds of blind patients were lower than those of some patients who were not blind (Fig. 3). These findings indicate that threshold of phosphenes rather than the visual acuity may be a better indicator of the residual RGC function in patients with severe retinal degeneration.

We further compared the thresholds in the group with a preservation of the central visual field left to those with a preservation of the peripheral visual field. Although the mean T1 threshold in the central visual field group was higher than that in peripheral visual field group, the mean T2 threshold in the central visual field group was not lower but higher than that in peripheral visual field group in spite of the remaining of the center of visual field (Fig. 4). Thus, the RGCs in the central retina were preserved more in the peripheral visual field group than in the central visual field group.

The mean current intensity of T1 and T2 in CRD patients was lower than those in RP patients (Fig. 5e), suggesting that the RGC function were more preserved in CRD patients than in RP patients in both the macula and extramacular areas.

Although all CRD patients showed a positive EEPRs, all RP patients did not show them. Moreover thresholds of phosphenes varied among RP patients. There were significant differences between the T1 and T2 for the group with an EEPR and those without an EEPR (Fig. 6). The presence or absence of EEPR is a good indicator of the extent of residual RGC function in patients with retinal degeneration.

On the contrary, the mean threshold of EEPR was twice as high as that of T2 in the group with an EEPR, although the thresholds of T2 and EEPR were close in normal subjects. Thus the thresholds of EEPR would not be a good indicator of the central phosphene in RP patients. A certain number of RGCs may have to be functioning to evoke a

pupillary constriction. However, in advanced RP patients, the density of RGC is so low that a higher current is needed to depolarize the widely scattered RGCs to evoke a pupillary constriction, while phosphene may be perceived even if a small number of RGCs were depolarized by TES.

These data suggest that three parameters, T1, T2 and P, measured by TES examination can be used to select candidates for retinal prostheses.

In summary, we have developed a safe method to elicit phosphenes and EEPR by TES to study the residual RGC function in patients with retinal degeneration. In RP patients, the presence of EEPR did not necessarily indicate the preservation of RGCs in the central retina, but reflected the overall activity of residual RGCs. Therefore, our method may provide information on the function of residual RGC which cannot be examined with currently available ophthalmologic instruments. Thus, among several tests required to select candidates for a retinal prosthesis [35],TES may have an important role.

Acknowledgements The authors thank Yozo Miyake, Satoshi Suzuki, Mineo Kondo and Yutaka Fukuda for advice and discussions.

References

1. Brindley GS (1955) The site of electrical excitation of the human eye. J Physiol 127:189–200
2. Chow AY, Chow VY (1997) Subretinal electrical stimulation of the rabbit retina. Neurosci Lett 225:13–16
3. Chow AY, Chow VY, Packo KH, Pollack JS, Peyman GA, Schuchard R (2004) The artificial silicon retina microchip for the treatment of vision loss from retinitis pigmentosa. Arch Ophthalmol 122:460–469
4. Delbeke J,Pins D, Michaux G, Wanet-Defalque MC, Parrini S, Veraart C (2001)Electrical stimulation of anterior visual pathways in retinitis pigmentosa. Invest Ophthalmol Vis Sci 42:291–297
5. Fariss RN, Li ZY, Milam AH (2000) Abnormalities in rod photoreceptors, amacrine cells, and horizontal cells in human retinas with retinitis pigmentosa. Am J Ophthalmol 129:215–223
6. Gebhard JW (1952) Thresholds of the human eye for electric stimulation by different wave forms. J Exp Psychol 44:132–140
7. Haruta M, Kosaka M, Kanegae Y, Saito I, Inoue T, Kageyama R, Nishida A, Honda Y, Takahashi M (2001) Induction of photoreceptor-specific phenotypes in adult mammalian iris tissue. Nat Neurosci 4:1163–1164
8. Hesse L, Schanze T, Wilms M, Eger M (2000) Implantation of retina stimulation electrodes and recording of electrical stimulation responses in the visual cortex of the cat. Graefe's Arch Clin Exp Ophthalmol 238:840–845
9. Humayun MS, Price M, de Juan Jr E, Barron Y, Moskowitz M, Klock IB, Milam AH (1999) Morphometric analysis of the extramacular retina from postmortem eyes with retinitis pigmentosa. Invest Ophthalmol Vis Sci 40:143–148
10. Humayun MS, Weiland JD, Fujii GY, Greenberg RJ, Williamson R, Little J, Mech B, Climmarusti V, Van Boemel G, Dagnelie G, de Juan Jr E (2003) Visual perception in a blind subject with a chronic microelectronic retinal prosthesis. Vision Res 43:2573–2581
11. Jensen RJ, Rizzo JF 3rd, Ziv OR, Grumet A, Wyatt J (2003) Thresholds for activation of rabbit retinal ganglion cells with an ultrafine, extracellular microelectrode. Invest Ophthalmol Vis Sci 44:3533–3543
12. Johnson LN, Guy ME, Krohel GB, Madsen RW (2000) Levodopa may improve vision loss in recent-onset, nonarteritic anterior ischemic optic neuropathy. Ophthalmology 107: 521–526
13. Kanda H, Morimoto T, Fujikado T, Tano Y, Fukuda Y, Sawai H (2004) Electrophysiological studies on the feasibility of suprachoroidal-transretinal stimulation for artificial vision in normal and RCS rat. Invest Ophthalmol Vis Sci 45:560–566
14. Kawasumi M (1985) Distribution of current intensities inside the electrically stimulated eye. Nippon Ganka Gakkai Zasshi 89:766–772
15. Li ZY, Kjavin IJ, Milam AH. (1995) Rod photoreceptor neurite sprouting in retinitis pigmentosa. J Neurosci 15:5429–5438
16. Majji AB, Humayun MS, Weiland JD, Suzuki S, D'Anna SA, de Juan Jr E (1999) Long-term histological and electrophysiological results of an inactive epiretinal electrode array implantation in dogs. Invest Ophthalmol Vis Sci 40:2073–2081
17. Margalit E, Maia M, Weiland JD, Greenberg RJ, Fujii GY, Torres G, Piyathaisere DV, O'Hearn TM, Liu W, Lazzi G, Dangnelie G, Scribner DA, de Juan Jr E, Humayun MS (2002) Retinal prosthesis for the blind. Surv Ophthalmol 47:335–356
18. Marmor MF, Aguirre G, Arden G (1983) Retinitis pigmentosa: a symposium on terminology and methods of examination. Ophthalmology 90: 126–131
19. Motokawa K, Iwama K (1950) Resonance in electrical stimulation of the eye. Tohoku J. Exp Med 53:201–206
20. Motokawa K, Ebe M (1952) Selective stimulation of color receptors with alternating currents. Science 25:115:92–94
21. Miyake Y, Yanagida K, Yagasaki K (1980) Clinical application of EER (electrically evoked response). (1) Analysis of EER in normal subjects. Nippon Ganka Gakkai Zasshi 84: 354–360
22. Miyake Y, Yanagida K, Yagasaki K (1980) Clinical application of EER (electrically evoked response) (2) Analysis of EER in patients with dysfunctional rod or cone visual pathway. Nippon Ganka Gakkai Zasshi 84:502–509

23. Pagon RA (1988) Retinitis pigmentosa. Surv Ophthalmol 33:137–177
24. Potts AM, Inoue J (1968) The electrically evoked response of the visual system (EER). Invest Ophthalmol 7:269–278
25. Potts AM, Inoue J (1969) The electrically evoked response of the visual system (EER) II. Effect of adaptation and retinitis pigmentosa. Invest Ophthalmol 8:605–613
26. Rizzo JF 3rd, Wyatt J, Loewenstein J, Kelly S, Shire D (2003) Perceptual efficacy of electrical stimulation of human retina with a microelectrode array during short-term surgical trials. Invest Ophthalmol Vis Sci 44: 5362–5369
27. Santos A, Humayun MS, de Juan E Jr, Greenberg RJ, Marsh MJ, Klock IB, Milam AH (1997) Preservation of the inner retina in retinitis pigmentosa: a morphometric analysis. Arch Ophthalmol 115:511–515
28. Schwahn HN, Gekeler F, Kohler K, Kobuch K, Sachs HG, Schulmeyer F, Jacob W, Gabel VP, Zrenner E (2001) Studies on the feasibility of a subretinal visual prosthesis: data from Yucatan micropig and rabbit. Graefe's Arch Clin Exp Ophthalmol 239:961–967
29. Stone JL, Barlow WE, Humayun MS, de Juan E Jr, Milam AH (1992) Morphometric analysis of macular photoreceptors and ganglion cells in retinas with retinitis pigmentosa. Arch Ophthalmol 110:1634–1639
30. Tanino T, Kato S, Kawasumi M (1981) Studies on electrically evoked pupillary reflex-Indirect reflex and its frequency characteristics. Jpn J Ophthalmol 25:423–429
31. Tanino T, Kurihara K (1982) Electrically evoked direct and consensual reflexs of the pupil. Jpn J Ophthalmol 26:462–467
32. Tanino T. (1982) Studies on electrically evoked pupillary reaction 1. Indirect electrical reaction and its frequency characteristic. Nippon Ganka Gakkai Zasshi (Japanese) 61:397–402
33. Veraart C, Raftopoulos C, Mortimer JT, Delbeke J, Pins D, Michaux G, Vanlierde A, Parrini S, Wanet-Defalque MC (1998) Visual sensations produced by optic nerve stimulation using an implanted self-sizing spiral cuff electrode. Brain Res 813:181–186
34. Walter P, Heimann K (2000) Evoked cortical potentials after electrical stimulation of the inner retina in rabbits. Graefe's Arch Clin Exp Ophthalmol 238:315–318
35. Yanai D, Lakhanpal RR, Weiland JD, Mahadevappa M, Van Boemel G, Fujii G, Greenberg R, Caffey S, de Juan Jr E (2003) The value of preoperative tests in the selection of blind patients for a permanent microelectronic implant. Trans Am Ophthalmol Soc 101: 223–230
36. Young MJ, Ray J, Whiteley RS, Klassen H, Gage FH (2000) Neuronal differentiation and morphological integration of hippocampal progenitor cells transplanted to the retina of immature and mature dystrophic rats. Mol Cell Neurosci 16:197–205

Jpn J Ophthalmol 2006;50:266–273

DOI 10.1007/s10384-005-0304-y

CLINICAL INVESTIGATION

Effect of Transcorneal Electrical Stimulation in Patients with Nonarteritic Ischemic Optic Neuropathy or Traumatic Optic Neuropathy

Takashi Fujikado[1], Takeshi Morimoto[1], Kenji Matsushita[2], Hiroshi Shimojo[2], Yoshitaka Okawa[1], and Yasuo Tano[2]

[1]Department of Applied Visual Science, Osaka University Graduate School of Medicine, Osaka, Japan; [2]Department of Ophthalmology, Osaka University Graduate School of Medicine, Osaka, Japan

Abstract

Purpose: To determine whether transcorneal electrical stimulation (TES) can improve the visual function of patients with nonarteritic ischemic optic neuropathy (NAION) or traumatic optic neuropathy (TON).

Methods: Eight consecutive patients at the Osaka University Hospital were studied. TES (600–800 μA, 20 Hz, 30 min) was applied once each to three eyes with NAION and to five eyes with TON, using a contact lens-type stimulating electrode. The primary outcome measurement was the change in visual acuity at 1 to 3 months after TES. An improvement in visual acuity was defined as a change of ≥0.3 log (minimum angle of resolution) (logMAR) units. The side effects of TES were also investigated.

Results: After TES application, the visual acuity improved in two patients with NAION and in four patients with TON. Visual acuity did not worsen in any of the eyes. Only a mild superficial punctuate keratopathy was observed in all eyes immediately after TES, and it healed by the next day.

Conclusions: Visual acuity can be improved after TES without major complications in some patients with NAION or TON. These results suggest that TES should be considered as a new treatment for eyes with optic neuropathy. **Jpn J Ophthalmol** 2006;50:266–273 © Japanese Ophthalmological Society 2006

Key Words: contact lens, electrical stimulation, neuroprotection, nonarteritic anterior ischemic neuropathy, traumatic optic neuropathy

Introduction

Nonarteritic ischemic optic neuropathy (NAION) and traumatic optic neuropathy (TON) are optic nerve diseases accompanied by a sudden decrease in vision.[1] The visual decrease is often severe, and there is no established treatment that can reverse the decrease.[1] The natural course of the changes in visual acuity in eyes with NAION was documented by the Ischemic Optic Neuropathy Decompression Trial (IONDT) study.[2] The percentage of patients with a recovery of ≥3 lines, 0.3 log (minimum angle of resolution) (logMAR) in visual acuity, was 39.7% at 3 months in a carefully followed-up group, but the visual acuity gradually decreased during the remainder of the follow-up period. The natural course of the visual recovery in eyes with TON was documented by the International Optic Nerve Trauma Study (IONTS).[3] The percentage of untreated patients with a recovery of ≥3 lines in visual acuity was 57% at 1 month and 50% at 3 months.

The definitive cause of NAION is unknown, but optic nerve head ischemia secondary to hypoperfusion by the short posterior ciliary arteries is suspected.[4] The IONDT study reported that optic nerve decompression surgery was not effective for treating NAION.[5] Recent studies have

Received: July 29, 2005 / Accepted: December 19, 2005
Correspondence and reprint requests to: Takashi Fujikado, Department of Applied Visual Science, Osaka University Graduate School of Medicine, 2-2 Yamadaoka, Suita, Osaka 565-0871, Japan
e-mail: fujikado@ophthal.med.osaka-u.ac.jp